



This discussion paper is/has been under review for the journal Geoscientific Instrumentation, Methods and Data Systems (GI). Please refer to the corresponding final paper in GI if available.

Background subtraction for the Cluster/CODIF plasma ion mass spectrometer

C. G. Mouikis, L. M. Kistler, G. Wang, and Y. Liu

Space Science Center, University of New Hampshire, Durham, New Hampshire, USA

Received: 18 April 2013 – Accepted: 4 July 2013 – Published: 27 September 2013

Correspondence to: C. G. Mouikis (chris.mouikis@unh.edu)

Published by Copernicus Publications on behalf of the European Geosciences Union.

Background subtraction for the Cluster/CODIF spectrometer

C. G. Mouikis et al.

[Title Page](#)

[Abstract](#)

[Introduction](#)

[Conclusions](#)

[References](#)

[Tables](#)

[Figures](#)

[⏪](#)

[⏩](#)

[◀](#)

[▶](#)

[Back](#)

[Close](#)

[Full Screen / Esc](#)

[Printer-friendly Version](#)

[Interactive Discussion](#)



2 Time-of-flight measurement

A significant advantage of the TOF sensors is the inherent coincidence requirement in the TOF measurement which reduces significantly the background contamination, as is demonstrated in Fig. 1. However, for TOF sensors, the foreground to background ratio is energy and species dependent. Assuming the same foreground fluxes for all energies and all species, particles with higher energy and lighter mass will have lower contamination levels.

Figure 2 shows an example (using preflight calibration data) of CODIF time-of-flight spectra for the four major ion species H^+ , He^{++} , He^+ and O^+ , at two representative energies, 40 keV e^{-1} (top panel) and 5 keV e^{-1} (bottom panel). The ion peaks appear as skewed Gaussian distributions. The tail towards longer times of flight is due to energy loss and scattering in the carbon foil. Time-of-flight windows for each species are defined so that the majority of the time-of-flight distribution for a particular species falls within the corresponding window. The start and end time of the TOF window for each species is marked with the vertical lines. The position and width of these TOF windows depends on the particle energy and mass; they are bunched closer together for the high energies and spread out for the lower energies. For both examples shown in Fig. 2, H^+ , He^+ and O^+ are easily separated while the He^{++} is in the tail of the H^+ distribution. In fact, the tails of the distribution of each species “spill” into the other species at a certain level. Table 1 shows the spillover fraction of the different species, for the two energies shown in Fig. 2, from pre-flight calibration data obtained from the high sensitivity side of S/C4. In order to assess the significance of the contamination level between species, the spillover fraction as well as the relative species abundance has to be considered. For example, inside the magnetosphere the He^{++} is almost irretrievable because the spillover from H^+ ($\sim 1.1\text{--}5.1\%$) is large compared to the real He^{++} signal. In contrast, the H^+ spillover into the O^+ TOF window is much lower ($\sim 0.1\text{--}0.3\%$) while the real O^+ counts are much higher inside the magnetosphere, which results in a much lower contamination level.

Background subtraction for the Cluster/CODIF spectrometer

C. G. Mouikis et al.

[Title Page](#)

[Abstract](#)

[Introduction](#)

[Conclusions](#)

[References](#)

[Tables](#)

[Figures](#)

[⏪](#)

[⏩](#)

[◀](#)

[▶](#)

[Back](#)

[Close](#)

[Full Screen / Esc](#)

[Printer-friendly Version](#)

[Interactive Discussion](#)



Background subtraction for the Cluster/CODIF spectrometer

C. G. Mouikis et al.

[Title Page](#)

[Abstract](#)

[Introduction](#)

[Conclusions](#)

[References](#)

[Tables](#)

[Figures](#)

[⏪](#)

[⏩](#)

[◀](#)

[▶](#)

[Back](#)

[Close](#)

[Full Screen / Esc](#)

[Printer-friendly Version](#)

[Interactive Discussion](#)



O^+ 3-D science data, under the assumption that during the radiation belt passes counts in this energy channel are all due to the penetrating relativistic electrons. One particular exception to this assumption is the presence of low energy field aligned O^+ populations frequently observed in the inner magnetosphere. Hence an extra precaution is taken.

The 180° instrument field of view is divided into 8 instrument anodes. How these 8 anodes and the spacecraft spin phase are combined to give the angle for the 3-D products is shown in Fig. 8 of Kistler et al. (2013). The background rate is deduced not from the counts registered in all the instrument anodes but from the counts registered in the two equatorial anodes, 4 and 5 (out of 8), only. This is because during the CLUSTER radiation belt encounters, the magnetic field is generally oriented along (or close to) the instrument z axis, in which case the two equatorial anodes are the ones that have the least chance to register counts from the field aligned populations.

3.2 Implementation

The implementation of this technique requires a number of steps. First, the exact time interval that the instrument registers background counts due to the radiation belt encounter has to be identified. Low energy O^+ populations are commonly observed during the inner magnetosphere passes and these intervals have to be distinguished from what is assumed to be background contamination. For example, such populations are evident in the O^+ energy spectra shown in Fig. 1 from 07:30 to 08:00 UT. The background interval selection is done visually using the O^+ energy spectra for each inner magnetosphere pass. The start and end times for each radiation belt encounter and for each spacecraft are stored in text files that are read by the background subtraction procedure. The dashed vertical lines in Fig. 3 indicate such an interval.

Next, the counts that are registered as O^+ in the lowest energy channel are converted into counts/second per TOF bin. This normalized background rate takes into account the number of TOF channels (bins) that correspond to the lowest energy channel O^+ and the integration time for this particular product. The background rate for the 18 April 2002 radiation belt encounter is shown in the bottom panel of Fig. 3. The top

Background subtraction for the Cluster/CODIF spectrometer

C. G. Mouikis et al.

[Title Page](#)

[Abstract](#)

[Introduction](#)

[Conclusions](#)

[References](#)

[Tables](#)

[Figures](#)

[⏪](#)

[⏩](#)

[◀](#)

[▶](#)

[Back](#)

[Close](#)

[Full Screen / Esc](#)

[Printer-friendly Version](#)

[Interactive Discussion](#)



panel in Fig. 4 shows an example of the angular distribution of the background contaminated data of a 3-D O^+ distribution. Each “globe” corresponds to a single instrument energy channel. The top left globe corresponds to the highest energy channel, while the bottom right globe corresponds to the lowest energy and will be used as the background monitor.

Assuming that all TOF channels, for all energies, register the same number of background counts, the background rate can be used to reconstruct the background contamination for each energy and each species. However, as was mentioned earlier, the two equatorial anodes have the least chance to register counts from actual field-aligned populations. Therefore, the average of the normalized counts deduced from the anodes 4 and 5 of the lowest energy O^+ channel will be used as the background rate instead. In order to convert this background rate into the background that the rest of the anodes would observe, the cross-anode efficiencies of the instrument for the radiation belt electrons are required. In Sect. 3.4, detailed information on how this is done, is provided.

From the deduced normalized background rate the background 3-D distributions can be reconstructed, for each species, for the whole time interval of the radiation belt encounter. Depending on the species that is being cleaned, the appropriate background 3-D distribution is reconstructed. First the background rate, determined from the O^+ , is interpolated to correspond with the time resolution for the particular species (different species/products can have different time resolution). Then, assuming that the background counts distribution is isotropic, the background counts are equally distributed on each anode over the corresponding angular bins (allowing for fractional counts). The middle panel in Fig. 4 shows the resulting background 3-D distribution for O^+ .

Finally, for each energy channel, the background distribution is subtracted from the original distribution (top panel) to produce the “cleaned” distribution (bottom panel). The resulting energy spectra are shown in Fig. 3a and b for H^+ and O^+ respectively. It is important to note that this subtraction can result in negative counts at the angular bin level. Both the foreground and background counts are distributed in a Poisson

Background subtraction for the Cluster/CODIF spectrometer

C. G. Mouikis et al.

[Title Page](#)

[Abstract](#)

[Introduction](#)

[Conclusions](#)

[References](#)

[Tables](#)

[Figures](#)

[⏪](#)

[⏩](#)

[◀](#)

[▶](#)

[Back](#)

[Close](#)

[Full Screen / Esc](#)

[Printer-friendly Version](#)

[Interactive Discussion](#)



distribution, so any count level N , has a statistical uncertainty of \sqrt{N} . Thus in regions that are background dominated, the subtraction will result in both positive and negative numbers due to the statistical variation. Those negative values are kept as is. Rejecting the negative values would “produce” artificial flux. It is important that a long time average reproduces the actual count rate for the particular interval. For example, this is shown in Fig. 3c where the “cleaned” counts for the lowest O^+ energy channel are plotted. The interval between the dashed lines was used to determine the background rate and by definition after the cleaning it should average to zero. A longer time average would show that indeed this is the case. In fact, we use this as a test against over/under subtraction.

3.3 Fine tuning the background rate

When the background rate deduced from the O^+ window TOF bins is applied to the H^+ background subtraction it becomes apparent that the normalized counts for a particular radiation background level is not the same for all the TOF bins. Early TOF bins (closer to the H^+ range) have higher background counts compared to the O^+ TOF bins and therefore an adjustment is needed for H^+ and He^+ .

For this reason, the 3-D distribution of background counts for each species is multiplied by a certain species dependent factor. The factor for O^+ is 1 (since O^+ is used to deduce the background level). For the other species, the factor was deduced by manually changing this factor and visually inspecting the cleaned energy spectrum. The variability of this factor was small and the values 1.65 and 1.2 were selected for H^+ and He^+ , respectively.

Subsequently, these factors were tested for selected events where it was evident (from visual inspection of the energy spectrograms) that the observed H^+ or He^+ counts at the lowest energy channels were only due to background. The requirement then was that after the background subtraction the average counts of the lowest energy channel are averaging to zero.

Background subtraction for the Cluster/CODIF spectrometer

C. G. Mouikis et al.

[Title Page](#)

[Abstract](#)

[Introduction](#)

[Conclusions](#)

[References](#)

[Tables](#)

[Figures](#)

[⏪](#)

[⏩](#)

[◀](#)

[▶](#)

[Back](#)

[Close](#)

[Full Screen / Esc](#)

[Printer-friendly Version](#)

[Interactive Discussion](#)



An additional step for the fine-tuning of the background subtraction is the use of the pitch angle spectra where background would appear as an isotropic population. Often, after the subtraction, strongly anisotropic populations are revealed that provide good reference points in deciding the exact level of background.

Finally, the “cleaned” counts are assigned an error bar based on the counting statistics for each time period that gives the statistical significance of the resulting fluxes. The relative error is calculated using:

$$\frac{\sqrt{C + C_b}}{C - C_b} \quad (1)$$

where C is the observed counts and C_b is the estimated background counts.

3.4 Radiation belt electron cross anode efficiencies

The determination of the response of each anode of the CODIF instrument to the relativistic electron radiation is necessary. Although the anode efficiencies for each ion species is known from the instrument calibrations, the anode response to the penetrating radiation belt electrons is not necessarily the same. Therefore, this response has to be determined in order to be able to convert the counts registered in the equatorial anodes 4 and 5 into the counts that the rest of the anodes would register.

Figure 5 shows the normalized counts registered in each anode (anode counts over total counts) for the lowest O^+ energy channel during the radiation belt pass on 18 April 2002. All anodes show an interval where the normalized response is flat, i.e., all anodes detected the same profile. This is an indication that these counts are solely due to the penetrating electrons. The level of this flat response, indicated by the dashed red lines, is different for each anode and indicates the different response of each anode. These levels are used to determine the cross anode efficiencies to the radiation belt electrons.

These cross anode efficiencies are deduced from the data once per month for the mission lifetime. If these efficiencies are not relatively accurate they will result in a non-

the assumption that in the plasma sheet all the observed He^{++} is due to spillover from the H^+ .

TOF spectra, as shown in Fig. 6, from the plasma sheet are accumulated for each year between 2001 and 2007. Such a TOF spectrum for one energy channel is shown in Fig. 7. Here, only a part of the TOF spectrum is shown. First the PHA data from the He^{++} TOF window and from a small TOF window after the He^+ , indicated by the two black line segments, are fitted with an exponential function ($y = h e^{(-x^d/\rho)} + c$). The resulting fit (dark blue line) provides the estimated tail of the H^+ distribution and the part of it that falls within the He^+ window is the estimated He^+ contamination. Next, the estimated contamination is subtracted from the He^+ TOF data (light blue), which results in the cleaned He^+ data (red line). The ratio of the estimated He^+ contamination counts over the registered He^{++} counts provides the percentage of He^{++} that spills in the He^+ TOF window. This percentage is calculated for each energy bin and for each year (using plasma sheet data only) and is shown in Fig. 8a.

Next, under the assumption that all the He^{++} observed is H^+ spillover, we use the science data to determine the H^+ percentage that spills in the He^{++} . Once more, this is done for each energy bin and for each year. The resulting ratios, shown in Fig. 8b, are the median values. The energy dependence for both ratios is the result of the dependence of the species TOF peak position on the particle energy. The width of the H^+ peak is dominated by electronic effects, and does not vary significantly with energy. Therefore, as the TOF peaks move closer together at higher energies (lower energy bins), there is more spillover. Finally, the product of these two ratios provides the percentage of H^+ that spills in the He^+ TOF window.

It is important to reiterate that the cleaned data set will have a higher statistical error because the accuracy of the density estimate depends strongly on the level of the background subtracted. At this point the spillover subtraction has been applied for the density moment. While it is possible to calculate the higher moments, the main point of this product is to extract He^+ when statistics are very low, so we are still testing whether valid higher order moments can be obtained in these situations. However, as

Background subtraction for the Cluster/CODIF spectrometer

C. G. Mouikis et al.

[Title Page](#)

[Abstract](#)

[Introduction](#)

[Conclusions](#)

[References](#)

[Tables](#)

[Figures](#)

[⏪](#)

[⏩](#)

[◀](#)

[▶](#)

[Back](#)

[Close](#)

[Full Screen / Esc](#)

[Printer-friendly Version](#)

[Interactive Discussion](#)



always, data analysis must be done intelligently, not blindly. A good check for whether the original data can be used would be to check the agreement between the “corrected” density and the “original” density. If agreement is good, then the subtraction is small and the rest of the moments should be valid.

5 Summary

We have presented two methods of background subtraction for the Cluster/CODIF instrument. The first method applies to background contamination due to penetrating electron radiation commonly occurring during the encounters with the Earth’s radiation belts and affects all species. Although TOF spectrometers, like CODIF, are relatively immune to background contamination due to the double coincidence requirement, high background rates can still result in false coincidences. A second type of background in these instruments occurs when events of one species, H^+ , fall into the time-of-flight range defined for another species, He^+ . Although the fraction of the H^+ events that spill into the He^+ measurement is small, when the actual He^+ fluxes are low this can result in significant contamination. Both techniques work well; however, when the signal to background ratio becomes small the statistical error of the resulting “cleaned” measurements is correspondingly large.

Acknowledgements. We are grateful to the many engineers and scientists from UNH, MPE, CESR, MPS, IFSI, IRF, UCB and UW who made the development of the CIS instrument possible. This work at UNH was supported by NASA under grant NNX11AB65G.

References

- Escoubet, C. P., Fehringner, M., and Goldstein, M.: *Introduction* The Cluster mission, Ann. Geophys., 19, 1197–1200, doi:10.5194/angeo-19-1197-2001, 2001.
- Kistler, L. M., Klecker, B., Jordanova, V. K., Möbius, E., Popecki, M. A., Patel, D., Sauvaud, J. A., Rème, H., Di Lellis, A. M., Korth, A., McCarthy, M., Cerulli, R., Bavassano Cattaneo, M. B.,

Background subtraction for the Cluster/CODIF spectrometer

C. G. Mouikis et al.

[Title Page](#)

[Abstract](#)

[Introduction](#)

[Conclusions](#)

[References](#)

[Tables](#)

[Figures](#)

[⏪](#)

[⏩](#)

[◀](#)

[▶](#)

[Back](#)

[Close](#)

[Full Screen / Esc](#)

[Printer-friendly Version](#)

[Interactive Discussion](#)



Background subtraction for the Cluster/CODIF spectrometer

C. G. Mouikis et al.

[Title Page](#)

[Abstract](#)

[Introduction](#)

[Conclusions](#)

[References](#)

[Tables](#)

[Figures](#)

[⏪](#)

[⏩](#)

[◀](#)

[▶](#)

[Back](#)

[Close](#)

[Full Screen / Esc](#)

[Printer-friendly Version](#)

[Interactive Discussion](#)



Eliasson, L., Carlson, C. W., Parks, G. K., Paschmann, G., Baumjohann, W., and Haerendel, G.: Testing electric field models using ring current ion energy spectra from the Equator-S ion composition (ESIC) instrument, *Ann. Geophys.*, 17, 1611–1621, doi:10.1007/s00585-999-1611-2, 1999.

5 Kistler, L. M., Mouikis, C. G., and Genestreti, K. J.: In-flight Calibration of the Cluster/CODIF sensor, *Geosci. Instrum. Method. Data Syst. Discuss.*, 3, 221–250, doi:10.5194/gid-3-221-2013, 2013.

10 Möbius, E., Kistler, L. M., Popecki, M. A., Crocker, K. C., Granoff, M., Jiang, Y., Sartori, E., Reme, H., Sauvaud, J.A., Cros, A., Aoustin, C., Camus, T., Medale, J.-L., Rouzaud, J., Carlson, C. W., McFadden, J. P., Curtis, D., Heeterks, H., Croyle, J., Ingraham, C., Klecker, B., Hovestadt, D., Ertl, M., Eberl, F., Kastle, H., Kunne, E., Laeverenz, P., Seidenschwang, E., Shelley, E. G., Klumpar, D. M., Hertzberg, E., Parks, G. K., McCarthy, M., Korth, A., Rosenbauer, H., Grave, B., Eliasson, L., Olsen, S., Balsiger, H., Schwab, U., and Steinacher, M.: The 3-D Plasma Distribution Function Analyzers With Time-of-Flight Mass Discrimination for Cluster, FAST, and Equator-S, in: *Measurement Techniques in Space Plasmas – Particles*, 102, edited by: Pfaff, R. F., AGU Geophysical Monograph, 102, 243–248, 1998.

15 Rème, H., Aoustin, C., Bosqued, J. M., Dandouras, I., Lavraud, B., Sauvaud, J. A., Barthe, A., Bouyssou, J., Camus, Th., Coeur-Joly, O., Cros, A., Cuvilo, J., Ducay, F., Garbarowitz, Y., Medale, J. L., Penou, E., Perrier, H., Romefort, D., Rouzaud, J., Vallat, C., Alcaydé, D., Jacquy, C., Mazelle, C., d’Uston, C., Möbius, E., Kistler, L. M., Crocker, K., Granoff, M., Mouikis, C., Popecki, M., Vosbury, M., Klecker, B., Hovestadt, D., Kucharek, H., Kuenneth, E., Paschmann, G., Scholer, M., Sckopke, N., Seidenschwang, E., Carlson, C. W., Curtis, D. W., Ingraham, C., Lin, R. P., McFadden, J. P., Parks, G. K., Phan, T., Formisano, V., Amata, E., Bavassano-Cattaneo, M. B., Baldetti, P., Bruno, R., Chionchio, G., Di Lellis, A., Mar-
20 cucci, M. F., Pallochia, G., Korth, A., Daly, P. W., Graeve, B., Rosenbauer, H., Vasyliunas, V., McCarthy, M., Wilber, M., Eliasson, L., Lundin, R., Olsen, S., Shelley, E. G., Fuselier, S., Ghielmetti, A. G., Lennartsson, W., Escoubet, C. P., Balsiger, H., Friedel, R., Cao, J.-B., Kovrazhkin, R. A., Papamastorakis, I., Pellat, R., Scudder, J., and Sonnerup, B.: First multi-
25 spacecraft ion measurements in and near the Earth’s magnetosphere with the identical Cluster ion spectrometry (CIS) experiment, *Ann. Geophys.*, 19, 1303–1354, doi:10.5194/angeo-19-1303-2001, 2001.

30 Wang, C.-P., Gkioulidou, M., Lyons, L. R., Wolf, R. A., Angelopoulos, V., Nagai, Weygand, J. M., and Lui, A. T. Y.: Spatial distributions of ions and electrons from the plasma sheet to

- the inner magnetosphere: Comparisons between THEMIS-Geotail statistical results and the Rice convection model, *J. Geophys. Res.*, 116, A11216, doi:10.1029/2011JA016809, 2011.
- Wüest, M.: Time-of-Flight Ion Composition Measurement Technique for Space Plasmas, in: *Measurement Techniques in Space Plasmas – Particles*, 102, edited by: Pfaff, R. F., AGU Geophysical Monograph, 102, 141–155, 1998.

5

Background subtraction for the Cluster/CODIF spectrometer

C. G. Mouikis et al.

[Title Page](#)

[Abstract](#)

[Introduction](#)

[Conclusions](#)

[References](#)

[Tables](#)

[Figures](#)



[Back](#)

[Close](#)

[Full Screen / Esc](#)

[Printer-friendly Version](#)

[Interactive Discussion](#)



Background subtraction for the Cluster/CODIF spectrometer

C. G. Mouikis et al.

Table 1. Spillover between species for 40 and 5 keV e⁻¹ particles from S/C 4 CODIF high sensitivity side pre-flight calibrations.

Energy (keV e ⁻¹)	Species	Spillover fraction in			
		H ⁺	He ⁺⁺	He ⁺	O ⁺
40	H ⁺		0.051	0.017	0.003
5	H ⁺		0.011	0.003	0.001
40	He ⁺⁺	0.286		0.165	0.009
5	He ⁺⁺	0.267		0.122	0.003
40	He ⁺	0.041	0.080		0.002
5	He ⁺	0.005	0.041		0.003
40	O ⁺	0.001	0.001	0.001	
40	O ⁺	0.002	0.0	0.002	

Title Page

Abstract

Introduction

Conclusions

References

Tables

Figures

⏪

⏩

◀

▶

Back

Close

Full Screen / Esc

Printer-friendly Version

Interactive Discussion

Background subtraction for the Cluster/CODIF spectrometer

C. G. Mouikis et al.

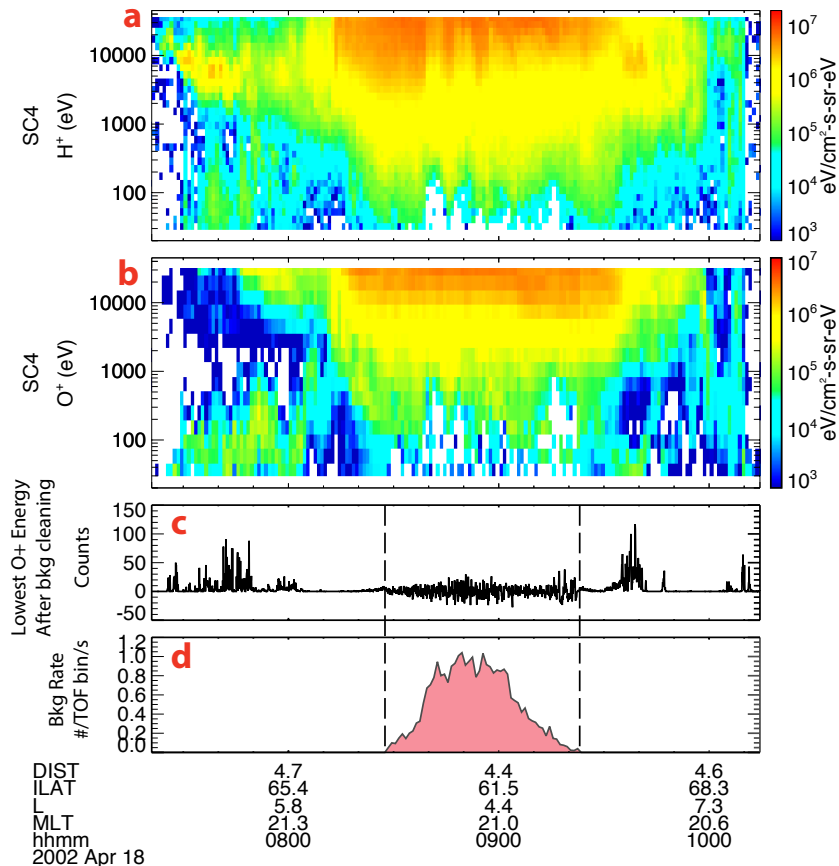


Fig. 3. Contamination subtracted H⁺ (a) and O⁺ (b) spectra. The dashed lines correspond to the interval that the background subtraction was applied. (c) shows counts in the lowest energy channel after the subtraction, which should average to zero. (d) shows the inferred background rate.

Title Page

Abstract Introduction

Conclusions References

Tables Figures

◀ ▶

◀ ▶

Back Close

Full Screen / Esc

Printer-friendly Version

Interactive Discussion



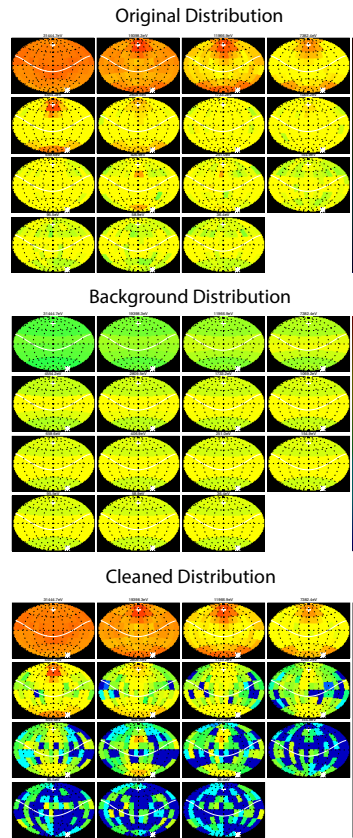


Fig. 4. Example of a contaminated O^+ distribution (top panel), the deduced background distribution and the resulted “cleaned” distribution. The individual “globes” correspond to the different energies with the top left globe corresponding to the highest energy channel and the bottom right globe corresponding to the lowest energy. Each globe shows the angular resolution in azimuthal and longitudinal directions.

Background subtraction for the Cluster/CODIF spectrometer

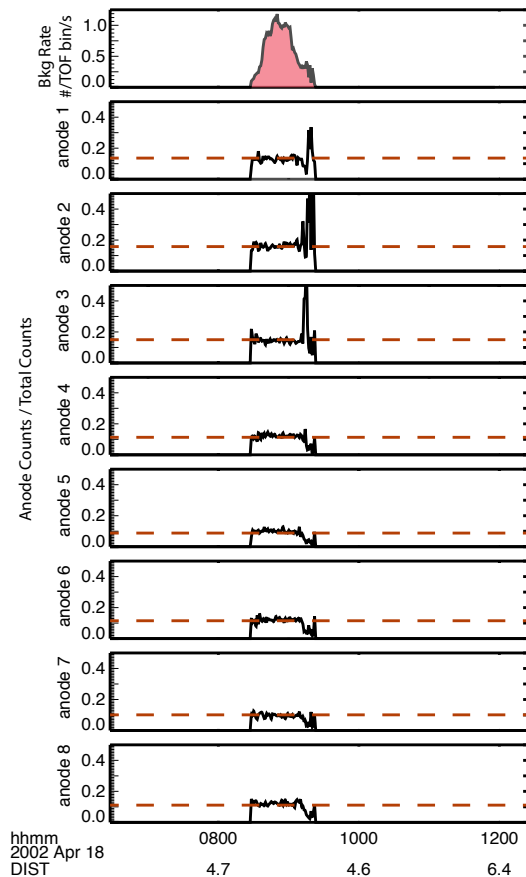
C. G. Mouikis et al.

Title Page	
Abstract	Introduction
Conclusions	References
Tables	Figures
⏪	⏩
◀	▶
Back	Close
Full Screen / Esc	
Printer-friendly Version	
Interactive Discussion	



**Background
subtraction for the
Cluster/CODIF
spectrometer**

C. G. Mouikis et al.

**Fig. 5.** Cross-anode efficiency determination of the penetrating electron response.[Title Page](#)[Abstract](#)[Introduction](#)[Conclusions](#)[References](#)[Tables](#)[Figures](#)[◀](#)[▶](#)[◀](#)[▶](#)[Back](#)[Close](#)[Full Screen / Esc](#)[Printer-friendly Version](#)[Interactive Discussion](#)

**Background
subtraction for the
Cluster/CODIF
spectrometer**

C. G. Mouikis et al.

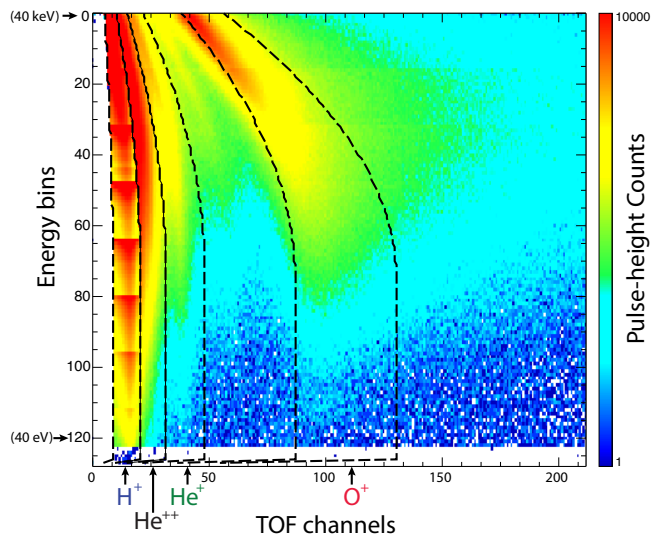


Fig. 6. CODIF time-of-flight spectrum for all energies. The dashed lines indicate the TOF windows for the four species, H⁺, He⁺⁺, H⁺ and O⁺.

[Title Page](#)[Abstract](#)[Introduction](#)[Conclusions](#)[References](#)[Tables](#)[Figures](#)[⏪](#)[⏩](#)[◀](#)[▶](#)[Back](#)[Close](#)[Full Screen / Esc](#)[Printer-friendly Version](#)[Interactive Discussion](#)

**Background
subtraction for the
Cluster/CODIF
spectrometer**

C. G. Mouikis et al.

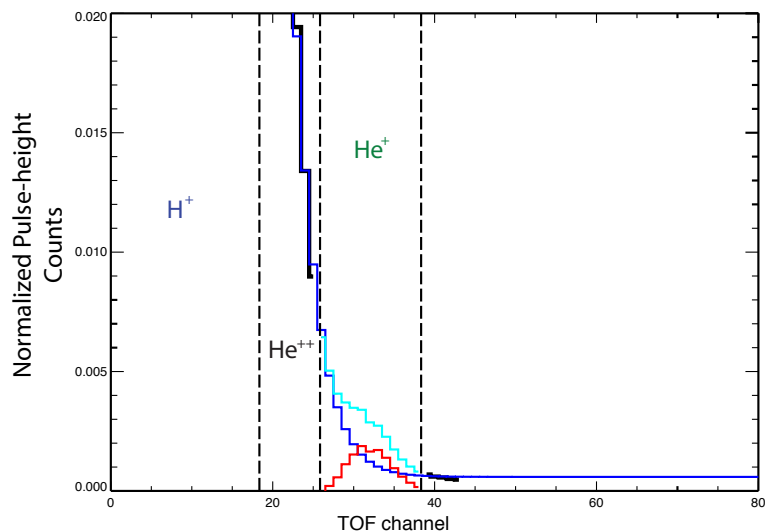


Fig. 7. Example of time-of-flight spectrum from a plasma sheet period. The dashed lines show the TOF windows for H^+ , He^{++} and He^+ . The black line together with the light blue line show the actual data. The light blue line indicates the registered counts in the He^+ channel. The blue line shows the fit to the two black line segments. The red line shows the subtracted counts in the He^+ window.

[Title Page](#)[Abstract](#)[Introduction](#)[Conclusions](#)[References](#)[Tables](#)[Figures](#)[⏪](#)[⏩](#)[◀](#)[▶](#)[Back](#)[Close](#)[Full Screen / Esc](#)[Printer-friendly Version](#)[Interactive Discussion](#)

Background subtraction for the Cluster/CODIF spectrometer

C. G. Mouikis et al.

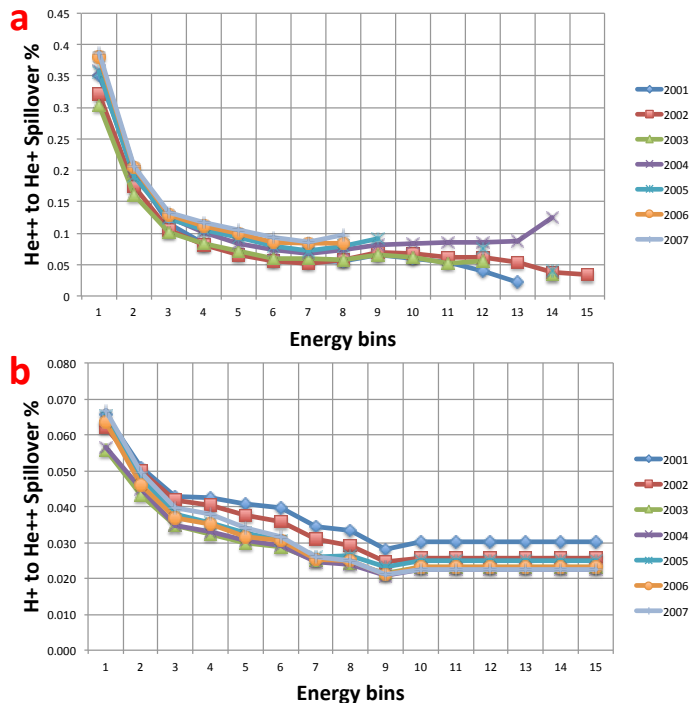


Fig. 8. (a) The He⁺⁺ percentage that spills in the He⁺ as a function of energy for the period 2001–2007. (b) The H⁺ percentage that spills in the He⁺⁺ as a function of energy for the same period. The percentage of the H⁺ counts that spill into the He⁺ is the product of the two percentage factors.